Eur. Phys. J. B **55**, 253–260 (2007)
DOI: 10.1140/epjb/e2007-00054-2

THE EUROPEAN PHYSICAL JOURNAL B

Anisotropic ferromagnetism induced in rutile single crystals by Co implantation

J.V. Pinto[1,3,4], M.M. Cruz[1,2,a], R.C. da Silva[3,4], N. Franco[3,4], A. Casaca[1,5] E. Alves[3,4], and M. Godinho[1,2]

[1] CFMC-Universidade de Lisboa, Campo Grande, Ed. C8, 1749-016 Lisboa, Portugal
[2] Dep. de Física, Faculdade de Ciências, Universidade de Lisboa, Campo Grande, Ed. C8, 1749-016 Lisboa, Portugal
[3] LFI, Dep. de Física, ITN, E.N.10 2686-953 Sacavém, Portugal
[4] CFNUL, Av.Prof.Gama Pinto 2, 1649-003 Lisboa, Portugal
[5] Instituto Superior de Engenharia de Lisboa, R. Cons. Emídio Navarro 1, 1950-062 Lisboa, Portugal

Received 19 July 2006 / Received in final form 16 January 2007
Published online 21 February 2007 –

Abstract. The magnetic and electrical properties of Co-implanted single crystalline TiO_2 rutile are presented. For fluences of the order of $10^{17}\,cm^{-2}$ and implantation energy of 150 keV the maximum atomic concentration of cobalt is 13 at% at a depth of 65 nm from the surface. The as implanted single crystals exhibit superparamagnetic behaviour attributed to the formation of nanosized cobalt clusters. After annealing at 1073 K an anisotropic ferromagnetic behaviour emerges with the easy magnetization axis lying in the (001) plane of rutile. The ferromagnetic behaviour is associated with oriented cobalt aggregates. Electrical conductivity of the implanted samples annealed in vacuum also exhibits anisotropic behaviour at low temperatures, but no magnetoresistive effects were detected.

PACS. 75.50.Tt Fine-particle systems; nanocrystalline materials – 61.72.Ww Doping and impurity implantation in other materials – 75.50.Dd Nonmetallic ferromagnetic materials – 75.50.Pp Magnetic semiconductors

1 Introduction

The recent discovery of magnetism coexisting with semiconductor type conductivity in oxides doped with magnetic ions [1] increased the interest in this type of materials due to their potential importance for spintronics applications. Cobalt doped TiO_2 has been extensively studied, both in anatase and rutile form [2,3], due to the prevalent ferromagnetic behaviour above room temperature (RT). Most of the work in these doped oxides has been carried out on films [4–22]. In these films the observed RT ferromagnetic behaviour (FM) varies largely, depending on the method of fabrication and growth conditions. There is still a debate regarding the origin of the FM and if it is possible to have a true diluted magnetic oxide character. In the case of anatase films, lower concentrations of cobalt seem to be associated with intrinsic magnetic behaviour while Co rich clusters appear for higher concentrations of the dopant [4–8] or films produced under low pressure of oxygen [4]. Aggregates are reported to be dissolved by annealing treatments [7,9]. For concentration values where cobalt rich clusters were detected other authors claim to find intrinsic magnetism [10,11]. Magnetoresistive effects were observed in films with low Co concentration [7] but FM was also reported in insulating films [12,13], indicating magnetic ordering in the absence of itinerant carriers. In the case of rutile films, the magnetic behaviour depends strongly on the oxygen pressure during growth [14] and annealing in vacuum increases FM [15]. Anomalous Hall effect was reported [16,17]. Clustering was observed to coexist with substitutional cobalt [18,19] and intrinsic FM [20], and was considered in some films to be the principal source of the RT-FM [14]. However, reported Magnetic Force Microscopy (MFM) measurements do not show evidence for the presence of aggregates [21,22]. The film/substrate interface seems to favour the nucleation of the aggregates [14,19]. The study of doped single crystalline samples overcomes the problems of interfaces and of the dimensional and induced stress restrictions present in films. Doping can be carried out using ion implantation. Results published recently for rutile implanted with cobalt, with a fluence of 1.5×10^{17} and $2\times10^{17}\,cm^{-2}$, and an energy of 40 keV, indicate anisotropic ferromagnetism and point to the possibility of intrinsic ferromagnetism [23–25]. From the implantation parameters presented by the authors [23] these results must have been obtained for high concentrations of cobalt (calculated to be in excess of 40 at.% in the maximum). The implanted concentration of cobalt in TiO_2 depends on the fluence and on the energy of implantation. Using higher implantation energy, 150 keV, and a

[a] e-mail: mmcruz@fc.ul.pt

fluence of the same order of magnitude, the dopant concentration can be reduced by factors of 2–3. For such a case, our previous results with maximum implanted concentrations of the order of 23 at.% [26] indicate that the magnetic behaviour is ferromagnetic and that metallic Co nanosized aggregates are formed. In this work the implanted cobalt concentration was further reduced by another factor of $\simeq$2 and the structural, electrical and magnetic characterization of TiO_2 rutile implanted crystals were carried out in order to clarify the origin of the observed magnetic behaviour

2 Experimental details

TiO_2 single crystalline plates cleaved in (100) orientation were implanted with Co, with fluences of 1×10^{17} cm^{-2}, at 150 keV implantation energy. Subsequent annealing treatments were carried out at 1073 K, for 1 h, in order to promote lattice recovery and rearrangement of the implanted ions. Some single crystals were annealed in vacuum, while others were annealed in air to study the influence of the reducing or oxidizing character of the atmosphere. Rutherford backscattering spectrometry (RBS), and RBS in combination with the channelling effect (RBS-C), performed with a 2 MeV $^4He^+$ beam, were used to follow the depth profiles of the implanted species, the recovery behaviour of the host lattice after the annealing treatments and the possible formation of new compounds. The backscattered particles were detected at 140° and close to 180° with two silicon solid state detectors of 13 keV and 16 keV energy resolution, respectively. X-ray diffraction was performed with a high resolution double crystal diffractometer, in a θ–2θ geometry. To characterize the magnetic behaviour of the samples, magnetic moment measurements were carried out using a Quantum Design MPMS magnetometer, for applied magnetic fields up to 5.5 T and temperatures between 2 K and 400 K. The magnetic moment as a function of temperature was measured in increasing temperature after cooling the samples from the highest temperature in zero field (zero field cooled — ZFC) or in the measurement field (field cooled — FC). For all implanted samples, two experimental geometries were used, with the external magnetic field parallel either to [010] or to [001] directions of rutile. In all cases, the magnetic moment results are interpreted as the sum of two independent contributions: a paramagnetic component assigned to the unimplanted TiO_2 and the contribution of the Co implanted region. The electrical conductivity of the implanted surface was measured as a function of temperature for both [010] and [001] directions, using a standard four-point method with in-line contacts. Magnetoresistance was also measured in the same geometries for applied magnetic fields up to 16 T.

TiO_2 rutile is a Van Vleck paramagnet. A careful characterization of the unimplanted single crystals, allowed us to determine an average magnetic susceptibility of 7.8×10^{-10} m^3/kg, similar along [010] and [001]. Since, in each case, the implanted depth corresponds to a very small fraction of the total sample volume (significantly less than 0.1%), the paramagnetic moment of the unimplanted region, essentially that of the bulk single crystal, is calculated using the measured susceptibility and the total mass. This contribution is always a major part of the measured experimental magnetic moment and is subtracted in the experimental results to isolate the contribution of the implanted region.

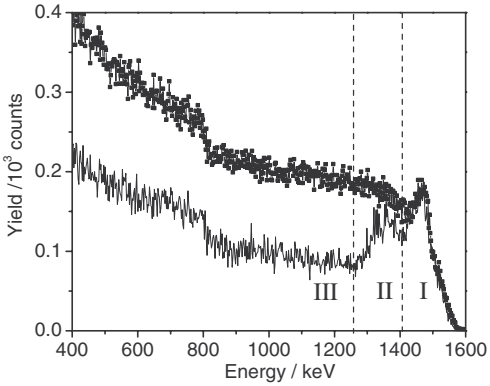

Fig. 1. RBS-C spectra for as-implanted sample: randomly oriented beam direction (squares) and [100] axial beam direction (solid line). The sections marked I, II and III correspond to contributions of the implanted cobalt and Ti implanted region, Ti in the implanted region and Ti in the bulk unimplanted region respectively.

3 Experimental results

3.1 As implanted samples

The RBS-C technique was used to extract the implantation profiles, the damage induced in TiO_2 host and the correlation of the implanted ions positions with the lattice sites. RBS spectra taken at a random and aligned incidence are presented in Figure 1.

Due to the similarity of Ti and Co masses, the RBS signal of cobalt is superimposed and mixed to some extent with the titanium contribution. In order to extract the Co depth profiles, spectra were obtained for different incidence angles and compared against theoretical simulations. The depth distributions were obtained from the theoretically generated spectra that better described the experimental data. This procedure allowed the conclusion that all samples have similar profiles, with maximum concentration of 13 at% at a depth of 65 nm from the surface. Under alignment conditions of the analyzing beam with the crystalline directions of the rutile single crystal, the ions get steered by the long range periodic potential of the lattice structure, and the RBS yield is dramatically reduced. This reduction in scattering yield is larger the better the crystalline quality of the steering host lattice. The high yield of the aligned spectra in the implanted region (II) versus unimplanted bulk region (III) indicates a strong dechannelling of the host rutile due to a highly damaged implanted region.

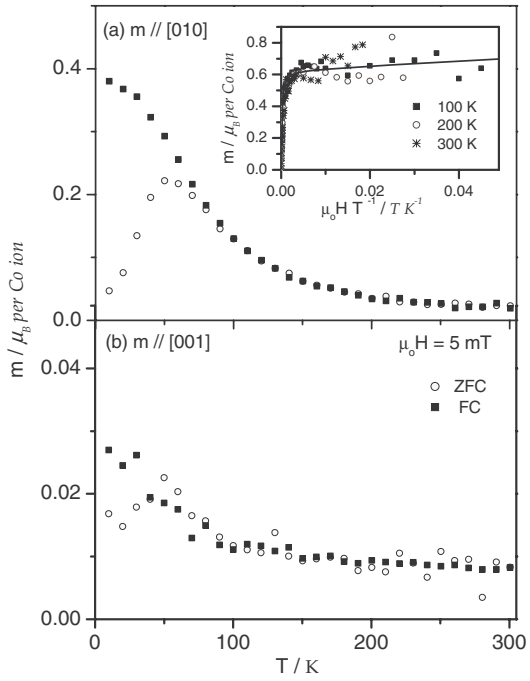

Fig. 2. ZFC-FC magnetic moment curves for as-implanted sample: (a) H ∥ [010]; (b)H ∥ [001].

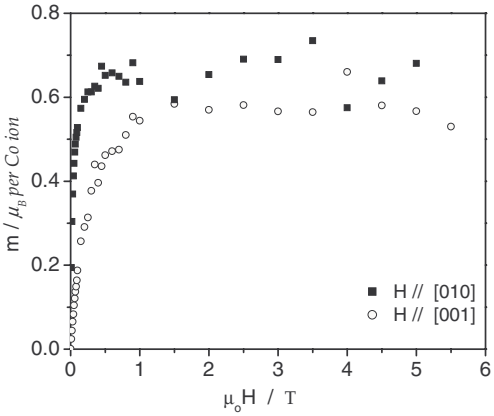

Fig. 3. Magnetic moment versus applied field at 100 K, in both axial directions for as-implanted sample.

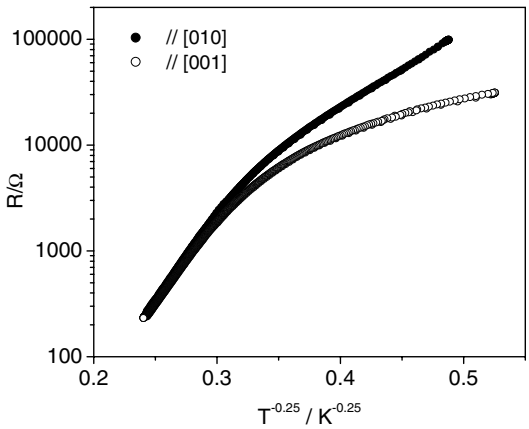

Fig. 4. Comparison between electrical resistance behaviour of as-implanted samples measured along both axial directions of rutile.

The magnetic moment dependence with temperature is displayed in Figure 2 and is characterized by the existence of a blocking temperature of 50 K above which the single crystals behave paramagnetically with huge magnetic moments. A simple Curie-Weiss fit results in a magnetic moment per implanted ion of the order of $100\mu_B$, a value that is too high to be assigned to an individual ion. This result indicates that the implanted samples are superparamagnetic, which is explained by the formation of Co rich nanosized aggregates behaving as magnetic single domains. This conclusion is supported by the scaling of the magnetic moment with H/T above 50 K (inset in Fig. 2a). The field dependence of the magnetic moment was measured in the two main non equivalent in-plane axial directions, [010] and [001], at 100 K and the data is presented in Figure 3. A saturation moment of $0.6\mu_B$ per implanted ion was determined for both directions. However, the initial slopes of the magnetization curves are clearly different, indicating that the nanosized aggregates display anisotropic behaviour, with an anisotropy that is related to the crystalline structure of rutile. This effect is also evident in the temperature dependence results, $m(T)$, shown in Figure 2. The conclusion is that the [001] direction of the rutile structure is a hard magnetization direction when compared to the direction parallel to [010]. A fit to the magnetic results using a log-normal volume distribution of metallic aggregates [29] and assuming uniaxial anisotropy gives an average magnetic moment per aggregate of $12000\mu_B$ with an anisotropy constant of $2.3 \times 10^5\,\mathrm{J\,m^{-3}}$. If these aggregates are considered of metallic cobalt, then they include 35% of the implanted cobalt and are characterized by an average diameter of 5.3 nm. Below the blocking temperature, hysteresis exists and coercive fields of 13 mT and 2.5 mT were determined at 10 K for applied fields parallel to the [010] and [001] TiO_2 directions, respectively.

To characterize the electric transport the electrical resistance was measured as a function of temperature. In agreement with previous results [26] the electrical resistivity exhibits 3D variable range hopping behaviour above 100 K (Fig. 4). Considering that both implanted Co ions and induced vacancies and interstitials act as impurities in the rutile gap, the behaviour of the electrical resistivity can be explained as due to an activated mobility of the carriers resulting from the disorder induced by implantation. The low electrical resistivity values at room temperature cannot be explained as an effect of implantation disorder alone [27] indicating that the implanted cobalt must play a significant role. As seen in Figure 4, only for temperatures below 90 K, the electrical resistivity exhibits anisotropic behaviour, increasing much faster along the [010] than along [001] direction, with decreasing temperature. Independently of the mechanism that determines the temperature dependence in this region, whether it is influenced by the ionization of impurities or involves

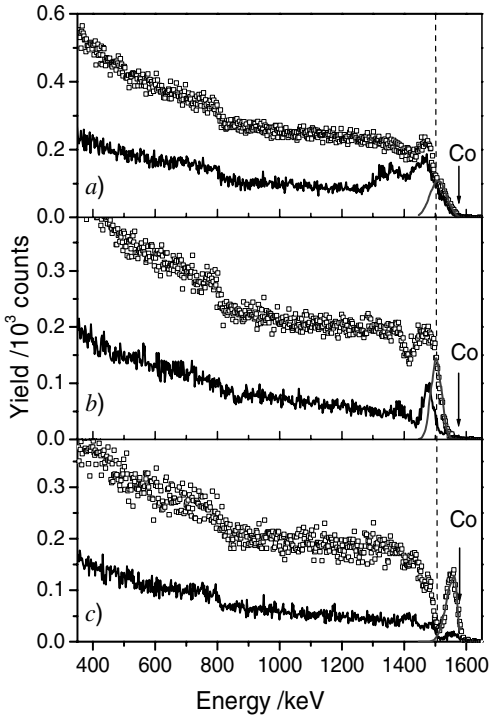

Fig. 5. RBS-C spectra taken in [100]-aligned (black line) and random (open squares) directions: (a) as-implanted; (b) annealed in vacuum; and (c) annealed in air. The grey lines show the implanted Co profiles extracted from the data. Clearly, the lattice recovery is accompanied by segregation of Co in-place (i.e. around the depth of maximum Co concentration, marked by the dashed line across the plot), or towards the surface, depending on the annealing environment, vacuum annealing or annealing in air, respectively.

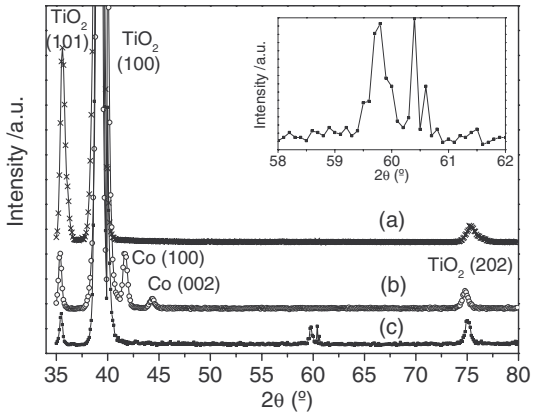

Fig. 6. XRD spectra for (a) as implanted sample; (b) annealed in vacuum at 1073 K; and (c) annealed in air at the same temperature.

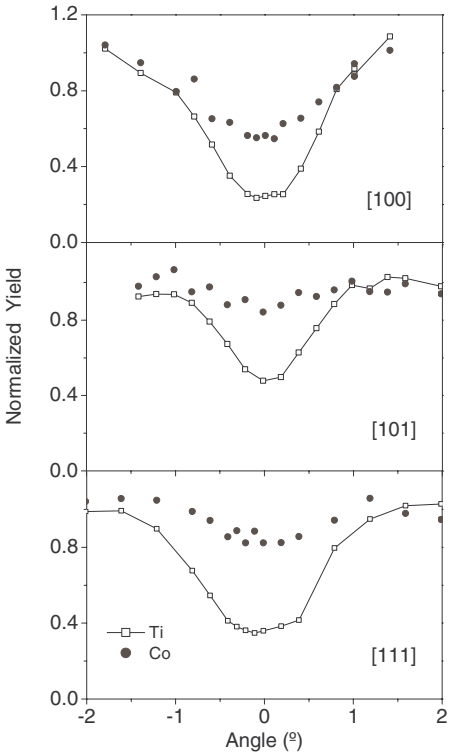

Fig. 7. Angular scans in the three principal axial directions for sample annealed in vacuum.

different variable range hopping paths, this result indicates that the mobility of the majority carriers is reduced in the [010] direction and that the electronic transport is strongly correlated with the rutile structure.

X-ray diffraction shows the presence of TiO_2 grains aligned with (101) plane parallel to the surface, while no evidence is found for the presence of metallic Co. This result can be explained by the small size of the aggregates and indicates that no definite orientation relationship with the host matrix is detected. Consistently, no channelling occurs in the implanted region in any of the major crystallographic directions.

3.2 Annealed samples

To recover the structure of rutile and induce rearrangement of the implanted cobalt, the samples were subjected to annealing treatments at 1073 K. The influence of reducing or oxidizing character of the annealing atmosphere was studied comparing samples annealed in vacuum with samples annealed in air under the same conditions. For samples annealed in vacuum, RBS results show that coalescence of the Co ions around the depth of maximum concentration was promoted, while in the samples annealed in air, the Co ions segregate to the surface (Fig. 5). It must be noted that the damage induced by the implantation procedure was significantly removed upon the thermal treatment in all cases, as the RBS aligned yields become significantly lower than for the as-implanted crystals.

In the case of vacuum annealed samples, the (101) TiO_2 grains almost disappear and metallic hcp Co is detected by X-ray diffraction (cf. Fig. 6), showing two different orientations parallel to the surface. To follow the accommodation of the cobalt ions in the oxide structure, RBS-C angular scans were performed trough the three principal rutile directions [100], [110] and [111] (Fig. 7).

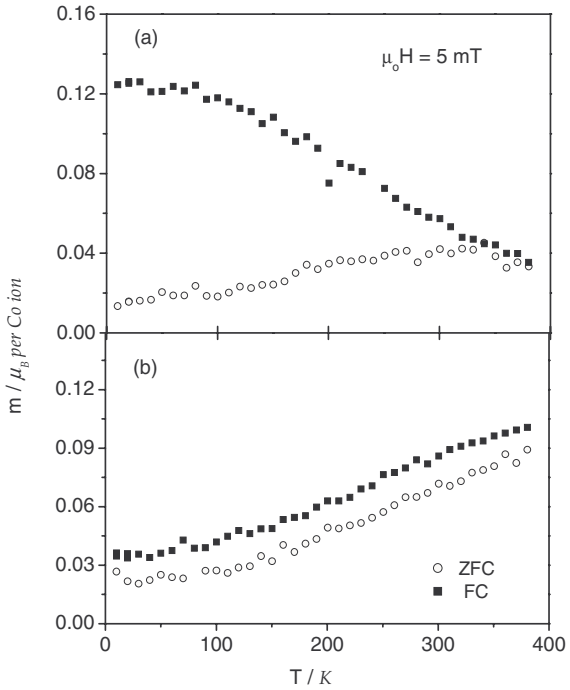

Fig. 8. ZFC-FC magnetic moment curves measured along the magnetic field in both directions for vacuum annealed sample. (a) H ∥ [010); (b) H ∥ [001].

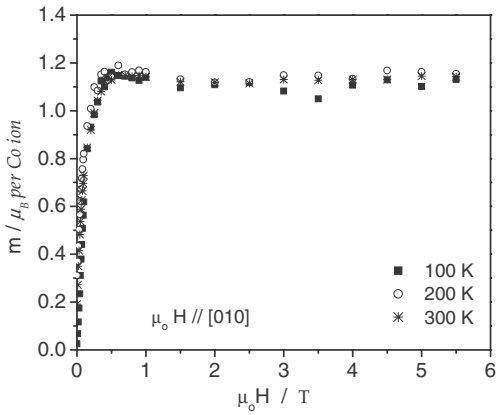

Fig. 9. Magnetic moment versus applied field for vacuum annealed sample measured in the easy magnetization [010] direction.

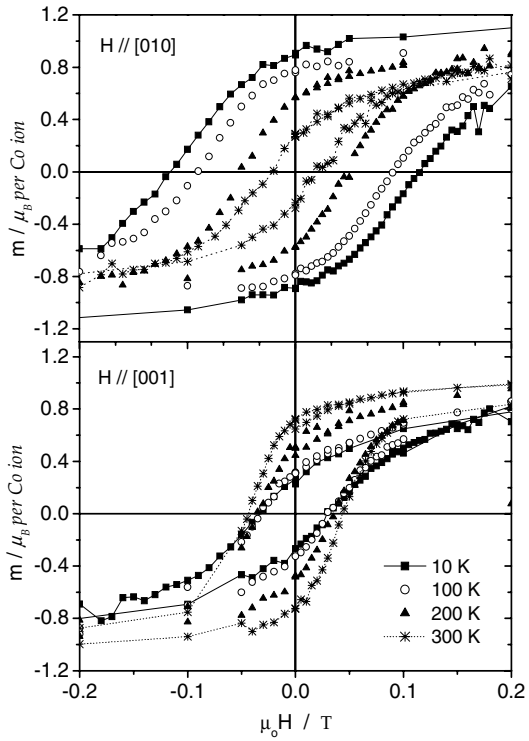

Fig. 10. Hysteresis loops taken at different temperatures in the hard and easy magnetization in-planar directions for vacuum annealed sample.

The results show different channelling yields for the Co ions, indicating some orientation relationship with the structure of the rutile lattice. The Co structures formed in the host rutile lattice must have preferential orientation along the [100] direction, since there is a clear correlated reduction of RBS-C yields along this direction.

For these samples, the magnetic moment results indicate that the magnetic behaviour becomes ferromagnetic like up to 350 K maintaining the strong anisotropic character correlated with the rutile structure (Figs. 8 and 9). A saturation moment of $1.2\mu_B$ per Co ion was determined in both directions, indicating an increased amount of Co in metallic aggregates as compared to the non annealed samples. Considering metallic cobalt aggregates and the same approximation as in the as implanted samples the average diameter of the aggregates is found to be 13 nm if the same anisotropy constant is considered or 8 nm if this constant is also allowed to vary increasing to a value of 4×10^5 J m^{-3}. Both these average diameters are obtained considering the temperature dependence of the magnetic moment only, since the high value of the blocking temperature does not allow the characterization of the superparamagnetic regime.

From both field and temperature dependence results the hard magnetization direction is still parallel to the [001] axis of rutile, after annealing. To test if part of the ferromagnetic behaviour could be associated with the increase of oxygen vacancies in reduced rutile, unimplanted crystals annealed in the same conditions were characterized. The crystals behave essentially as Van Vleck paramagnets with an increase of the rutile susceptibility value by a factor around 10% and do not exhibit ferromagnetic behaviour.

Hysteresis loops at different temperatures were obtained for both directions [010] and [001] and are presented in Figure 10. The dependence of the coercive field with temperature for the [010] direction supports the conclusion that the magnetic behaviour is associated with nanosized aggregates. From the coercive field values measured with the magnetic field applied along the easy magnetization direction, [010], assuming uniaxial anisotropy and the saturation magnetization of cobalt, an anisotropy constant of 2×10^5 J m^{-3} and a blocking temperature of 450 K

were deduced using

$$H_c = K_{eff}/\mu_o M_{sat}(1 - (T/T_B)^{0.5}) \quad (1)$$

K_{eff}, M_{sat} and T_B corresponding to the effective magnetic anisotropy constant, the cobalt saturation magnetization and the blocking temperature, respectively [28]. These values agree with the parameters obtained from the ZFC magnetic moment fit using a log-normal volume distribution of aggregates. The value of the anisotropy constant is of the same order of magnitude as in metallic cobalt ($K_1 = 7 \times 10^5$ J m^{-3} at temperatures lower than 200 K, decreasing to 2×10^5 J m^{-3} at 400 K) and indicates that the surface anisotropy is not the major contribution for the magnetic anisotropy of the aggregates. The orientation of the aggregates is nevertheless determined by the rutile structure since RBS/channelling indicates coherence between the Co positions and the lattice along the [100] axis.

The electrical resistivity of the implanted crystals after annealing are presented in Figure 11. The results obtained along [010] are characteristic of a doped semiconductor behaviour, displaying a strong decrease at low temperatures, associated with the ionization of impurities followed by a non-linear increase at higher temperatures due to the temperature dependence of mobility. The general behaviour along the [001] direction is similar, but the electrical resistivity increases almost linearly above 100 K. Since it is known that rutile becomes a semiconductor as a consequence of reduction, unimplanted crystals were annealed in the same conditions and the electrical resistance measured along the same directions with exactly the same distance between contact points. The results are shown in Figure 11 and indicate that in fact rutile has a semiconductor like behaviour displaying anisotropy in the electric conduction. Nevertheless, for the implanted samples, the electrical resistance is lower and the anisotropy increases.

To study the effect of the magnetic field in the electronic transport, resistance was measured along the same directions in an applied magnetic field up to 16 T. No magnetoresistive effects were detected in either of the two directions (Fig. 12).

In the case of samples annealed in air, major differences were detected as compared to samples annealed in vacuum. The RBS results indicate that cobalt diffuses to the surface while X-ray diffraction shows no indication of the presence of metallic cobalt. Instead, there are two X-ray diffracted lines at 2θ values of 59.7° and 60.4° that may be associated with a cobalt rich oxide formed at the surface (cf. inset in Fig. 6). A decrease in the number of (101) TiO_2 grains is also detected. The samples become essentially paramagnetic, the saturation magnetization decreasing to $0.03\mu_B$ per Co ion (Fig. 13), and the electrical resistance of the implanted layer increases above the experimental limit of our system and thus it could not be measured. Since cobalt diffused to the surface which becomes non conducting, consistently with Co being in a non metallic state, a Co rich compound, probably an oxide, is assumed to be formed.

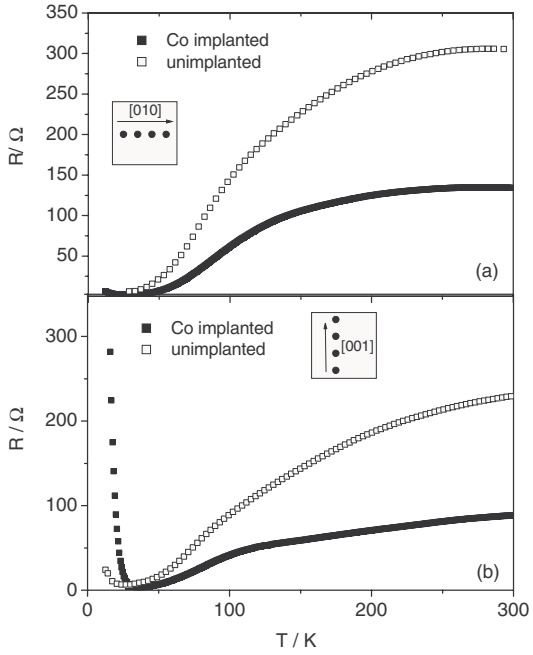

Fig. 11. Comparison between electrical resistance behaviour of unimplanted and Co implanted samples, after vacuum annealing, in both in plane directions of rutile: (a) [010]; (b) [001].

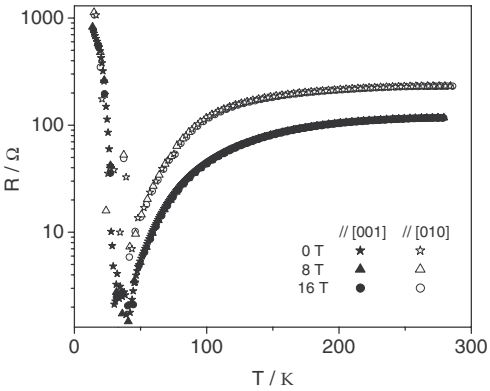

Fig. 12. Electrical resistance in applied magnetic field for Co implanted samples measured with the contacts aligned in the two directions referred in the text: open symbols [010], full symbols [001]. No differences can be detected between the resistance values measured in zero applied magnetic field or in applied magnetic fields up to 16 T.

4 Discussion and conclusions

The experimental results indicate that nanosized Co clusters are formed directly by the ion implantation of cobalt into rutile. The size of these aggregates depends on the local implanted concentration. In fact, in earlier work with 23 at.% local concentration, precipitates were found to have an average diameter of 11 nm [26], while in the present case for a local concentration of 13 at.% an average diameter of 5.3 nm is found. The metallic cobalt aggregates are oriented in the rutile structure and display magnetic anisotropy with the easy magnetization axis being in the basal plane of rutile.

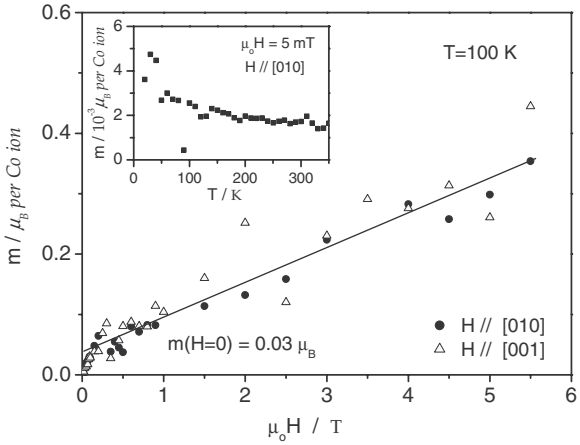

Fig. 13. Magnetic moment versus applied field for air annealed sample measured in both [010] and [001] directions. The inset illustrates the magnetic moment temperature dependence measured at 5 mT.

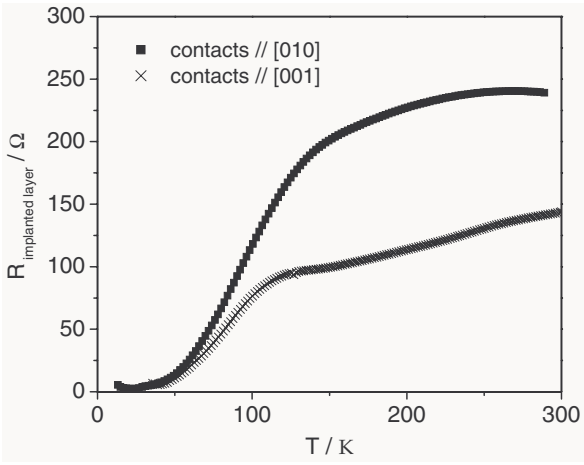

Fig. 14. Electrical resistance deduced for the implanted layer contribution using the model described in the text.

Annealing in vacuum induces growth of these precipitates in the implanted region that display anisotropic ferromagnetic like behaviour.

Annealing in air promotes the segregation of cobalt to the surface of rutile. This result indicates that the aggregates are not stable under an oxidizing atmosphere and points to a major role of the oxygen vacancies in stabilizing the aggregates in reduced rutile. One possible mechanism is the accommodation of vacancies at the interface between the aggregates and the TiO_2 host, consistent with the fact that the magnetic anisotropy constant is close to the bulk cobalt value and has a small contribution of the surface. Removal of the oxygen vacancies in an oxidizing environment prevents the stability of the aggregates and pushes Co out of the rutile structure.

The magnetic aggregates were identified by XRD analysis as hcp cobalt having two different orientations: $(002)_{\mathrm{Co}} \parallel (100)_{rutile}$ and $(100)_{\mathrm{Co}} \parallel (100)_{rutile}$. Considering that the aggregates are hcp and the direction of easy magnetization is parallel to the c-axis of hcp Co, we can correlate the orientation of these clusters with the rutile directions. As the easy direction of magnetization was detected parallel to the [010] direction of rutile single crystals, the Co clusters must have the c axis aligned parallel to this rutile direction, consistently with the XRD observation of aggregates with $(100)_{\mathrm{Co}} \parallel (100)_{rutile}$. The existence of a second orientation (002) in XRD can then be explained by the equivalence between [100] and [010] directions of rutile, that implies the existence of Co clusters with the c-axis parallel to the [100] direction of rutile and then $(001)_{\mathrm{Co}} \parallel (100)_{rutile}$. Both orientations are consistent with having the easy axis direction of hcp cobalt normal to the [001] direction of rutile and explain why this direction is a hard direction of magnetization.

The electrical behaviour of the samples is strongly determined by the reduction of rutile. For reduced rutile, published results indicate that one of the major carrier sources is the presence of Ti interstitials that become ionized above about 4 K [30]. The electrical resistance of the unimplanted crystals is explained in the same way: electrical transport occurs in two conduction bands separated by a gap of the order of 40 meV, the contribution of the upper band, more anisotropic, coming into play around 100 K. To understand the role of the cobalt implanted layer and since the resistance is measured in the narrow implanted region laying above a reduced rutile, a model was assumed where the resistance of the implanted samples is considered as resulting from the parallel transport between the implanted surface layer and the underneath reduced rutile.

Considering the experimental results for the unimplanted samples as accounting for the resistance of reduced rutile, the implanted layer contribution was extracted using $1/R_{impl} = 1/R - 1/R_{unimpl}$. These results are plotted in Figure 14. Clearly the electrical transport is anisotropic and related with the rutile lattice. Results indicate that the electrical resistance follows the same trends as the one of reduced rutile implying that conduction proceeds through the bands of rutile with a larger number of carriers. The change of behaviour at 100 K is associated with the enhanced conduction in the upper band, that also explains the increase in anisotropy. Implantation of cobalt increases conductance and the ionization energies of the carriers in the implanted sample extends to higher values than the ones in reduced rutile, since the low temperature activated regime shifts to higher temperatures. The question remains if the implanted cobalt acts as a source of carriers or if the increase in conductivity is simply related with an increased concentration of oxygen vacancies around the aggregates.

The absence of magnetoresistive effects indicates that there are no polarization effects of the charge carriers induced by the presence of cobalt ions.

This work is partially supported by the Portuguese foundation FCT through the Ph.D. grant (BD/8907/2002) to J.V. Pinto.

Note added in proof

After the submission of the present work, the authors learned that results of spin polarization were published for TiO_2 rutile implanted with $1.5 \times 10^{17}\,cm^{-2}$ and implantation energy of 40 keV [A. Nefedov, N. Akdogan, H. Zabel, R.I. Khaibulin, L.R. Tagirov, Appl. Phys. Lett. **89**, 182509 (2006)]. Spin polarization of oxygen associated with the presence of the implanted cobalt is reported for samples with implanted concentrations higher than the ones reported in this paper.

References

1. Y. Matsumoto, M. Murakami, T. Shono, T. Hasegawa, T. Fukumura, M. Kawasaki, P. Ahmet, T. Chikyow, S. Koshihara, H. Koinuma, Science **291**, 854 (2001)
2. T. Fukumura, H. Toyosaki, Y. Yamada, Semicond. Sci. Technol. **20**, S103 (2005)
3. R. Janisch, P. Gopal, A. Spaldin, J. Phys.: Condens. Matter **17**, R657 (2005)
4. D.H. Kim, J.S. Yang, K.W. Lee, S.D. Bu, T.W. Noh, S.-J. Oh, Y.-W. Kim, J.-S. Chung, H. Tanaka, H.Y. Lee, T. Kawai, Appl. Phys. Lett. **81**, 2421 (2002)
5. N.-J. Seong, S.-G. Yoon, C.-R. Cho, Appl. Phys. Lett. **81**, 4209 (2002)
6. S. Guha, K. Ghosh, J.G. Keeth, S.B. Ogale, S.R. Shinde, J.R. Simpson, H.D. Drew, T. Venkatsen, Appl. Phys. Lett. **83**, 3296 (2003)
7. S.R. Shinde, S.B. Ogale, S. Das Sarma, J.R. Simpson, H.D. Drew, S.E. Lofland, C. Lanci, J.P. Buban, N.D. Browning, V.N. Kulkarni, J. Higgins, R.P. Sharma, R.L. Green, T. Venkatsen, Phys. Rev. B **67**, 115211 (2003)
8. G.C. Han, P. Luo, Z.B. Guo, F.U. Nahar, M. Tay, Y.H. Wu, S.J. Wang, Thin Solid Films **505**, 137 (2006)
9. V.N. Kulkarni, S.R. Shinde, Y.G. Zhao, R.J. Choudhary, S.B. Ogale, R.L. Greene, T. Venkatesan, Nucl. Inst. Methods B **219–220**, 902 (2004)
10. N.H. Hong, J. Sakai, W. Prellier, A. Hassini, A. Ruyter, F. Gervais, Phys. Rev. B **70**, 195204 (2004)
11. N.H. Hong, W. Prellier, J. Sakai, A. Ruyter, J. Phys.: Condens. Matter **16**, 5549 (2004)
12. K.A. Griffin, A.B. Pakhomov, C.M. Wang, S.M. Heald, K.M. Krishnam, Phys. Rev. Lett. **94**, 157204 (2005)
13. T. Zhao, S.R. Shinde, S.B. Ogale, H. Zheng, T. Venkatesan, R. Ramesh, S. Das Darma, Phys. Rev. Lett. **94**, 126601 (2005)
14. D.H. Kim, K.W. Lee, J.S. Yang, T.W. Noh, S.D. Bu, Y.-W. Kim, R. Jung, J. Korean, Phys. Soc. **46**, 503 (2005)
15. R. Suryanarayanan, V.M. Naik, P. Kharel, P. Talagala, R. Naik, Solid State Comm. **133**, 439 (2005)
16. J.S. Higgins, S.R. Shinde, S.B. Ogale, T. Venkatesan, R.L. Green, Phys. Rev. B **69**, 073201 (2004)
17. S.R. Shinde, S.B. Ogale, J.S. Higgins, H. Zheng, A.J. Millis, V.N. Kulkarni, R. Ramesh, R.L. Greene, T. Venkatesan, Phys. Rev. Lett. **92**, 166601 (2004)
18. A. Punnoose, M.S. Seehra, W.K. Park, J.S. Moodera, J. Appl. Phys. **93**, 7867 (2003)
19. A.K. Pradhan, D.Hunter, J.B. Dadson, T.M. Williams, K. Zhang, K. Lord, B. Lasley, R.R. Rakhimov, J. Zhang, D.J. Sellmyer, U.N. Roy, Y. Chui, A. Burger, C. Hopkins, N. Pearson, A.L. Wilkerson, Appl. Phys. Lett. **86**, 222503 (2005)
20. M. Murakami, Y. Matsumoto, T. Hasegawa, P. Ahmet, K. Nakajima, T. Chikyow, H. Ofuchi, I. Nakai, H. Koinuma, J. Appl. Phys. **95**, 5330 (2004)
21. N.H. Hong, W. Prellier, J. Sakai, A. Ruyter, J. Appl. Phys. **95**, 7378 (2004)
22. N.H. Hong, J. Sakai, W. Prellier, A. Hassini, Appl. Phys. Lett. **83**, 3129 (2003)
23. R.I. Khaibullin, L.R. Tagirov, B.Z. Rameev, Sh. Z. Ibragimov, F. Yildiz, B. Aktas, J. Phys.: Condens. Matter **16**, L443 (2004)
24. N. Akdogan, B.Z. Rameev, L. Dorosinsky, H. Sozeri, R.I. Khaibullin, B. Aktas, L.R. Tagirov, A. Westphalen, H. Zabel, J. Phys.: Condens. Matter **17**, L359 (2005)
25. N. Akdogan, B.Z. Rameev, R.I. Khaibullin, A. Westphalen, L.R. Tagirov, B. Aktas, H. Zabel, J. Magn. Magn. Mater. **300**, e4 (2006)
26. J.V. Pinto, M.M. Cruz, R.C. da Silva, E. Alves, M. Godinho, J. Magn. Magn. Mat. **294**, e73 (2005)
27. O. Meyer, I. Khubeis, R. Fromknecht, S. Massing, Nucl. Instr. Meth. B **127/128**, 624 (1997)
28. J.L. Dormann, D. Fiorani, E. Tronc, Adv. Chem. Phys. **98**, 283 (1977)
29. J.V. Pinto, M.M. Cruz, R.C. da Silva, E. Alves, R. González, M. Godinho, Eur. Phys. J. B **45**, 331 (2005)
30. E. Yagi, R.R. Hasiguti, M. Aono, Phys. Rev. B **54**, 7945 (1996)